

Thermoelastic dynamic analysis of wavy carbon nanotube reinforced cylinders under thermal loads

Rasool Moradi-Dastjerdi^{*1} and Gholamhassan Payganeh²

¹Department of Mechanical Engineering, Khomeinishahr Branch, Islamic Azad University, Khomeinishahr, Iran

²Department of Mechanical Engineering, Shahid Rajaei Teacher Training University (SRTTU), Tehran, Iran

(Received April 15, 2017, Revised July 01, 2017, Accepted July 10, 2017)

Abstract. In this work, thermoelastic dynamic behavior of functionally graded carbon nanotube reinforced composite (FG-CNTRC) cylinders subjected to mechanical pressure loads, uniform temperature environment or thermal gradient loads is investigated by a mesh-free method. The material properties and thermal stress wave propagation of the nanocomposite cylinders are derived after solving of the transient thermal equation and obtaining of the time history of temperature field of the cylinders. The nanocomposite cylinders are made of a polymer matrix and wavy single-walled carbon nanotubes (SWCNTs). The volume fraction of carbon nanotubes (CNTs) are assumed variable along the radial direction of the axisymmetric cylinder. Also, material properties of the polymer and CNT are assumed temperature-dependent and mechanical properties of the nanocomposite are estimated by a micro mechanical model in volume fraction form. In the mesh-free analysis, moving least squares shape functions are used to approximate temperature and displacement fields in the weak form of motion equation and transient thermal equation, respectively. Also, transformation method is used to impose their essential boundary conditions. Effects of waviness, volume fraction and distribution pattern of CNT, temperature of environment and direction of thermal gradient loads are investigated on the thermoelastic dynamic behavior of FG-CNTRC cylinders.

Keywords: thermoelastic dynamic analysis; thermal gradient loads; wavy carbon nanotubes; nanocomposite cylinders; mesh-free

1. Introduction

Carbon nanotubes have attracted considerable academic and industrial interest because of multifarious nanotechnology applications. This is due to their extraordinary thermoelastic and physical properties that make them suitable candidates for reinforcement in nanocomposites (Kundalwal and Ray 2011). Some investigations have shown that the addition of small amount of CNT in the matrix can successfully improve thermal and mechanical properties of CNT base nanocomposite (Mokashi *et al.* 2007, Qian *et al.* 2000, Zhu *et al.* 2007).

Also, the effects of CNT characteristics (such as: aspect ratio, waviness, agglomeration and etc) on the reinforcement behavior of CNT/epoxy composite are studied (Kundalwal and Meguid 2015, Martone *et al.* 2011, Ray and Kundalwal 2014, Yazdchi and Salehi 2011). Kundalwal and Ray 2013 used mechanics of materials approach to estimate effective elastic properties of the fuzzy fiber reinforced composite (FFRC) and showed that axial effective elastic properties of FFRC containing wavy CNTs can be improved over those of FFRC with straight CNTs.

The effect of wavy CNTs on thermoelastic properties of short FFRC is examined by Kundalwal and Ray (2014) and they revealed that effective values of the thermal expansion

coefficients of the short FFRC are temperature dependant. Kundalwal *et al.* 2014 introduced a fuzzy carbon fiber heat exchanger (FFHE) with sinusoidally wavy CNTs on hollow cylindrical carbon fiber and reported that effective axial thermal conductivity of the FFHE significantly improves over that of bare hollow cylindrical carbon fiber heat exchanger.

Functionally graded materials (FGMs) are novel multi-phase composite materials with gradient phase volume fraction variations in space, in specific profile(s). They are mainly employed to withstand elevated temperatures and severe thermal gradients (Shariyat *et al.* 2010). Recently, the distribution of reinforcement phase is varied spatially according to a certain direction by considering of the concept of FGMs. So, several works on FGMs and functionally graded CNTRC structures were carried out. Sladek *et al.* 2007 used meshless local Petrov-Galerkin method (MLPG) for analysis of transient heat conduction in 3-D axisymmetric FGM cylinders. Golbahar Haghighi *et al.* 2009 presented a procedure for 3-D transient inverse heat conduction to estimate the unknown boundary heat flux of FGM plates. Sofiyev (2010) developed an analytical study based on the theory of vibrations of cylindrical shells for dynamic analysis of infinite length FGM cylindrical shell subjected to moving loads with constant velocity. The nonlinear thermo-elastic, vibration, and stress wave propagation behaviors of FGM cylinders are analyzed by Shariyat *et al.* (2010) based on a third-order Hermitian finite element formulation. Zhao and Liew (2010) presented buckling behavior of functionally graded cylindrical shell

*Corresponding author, Ph.D.,
E-mail: rasoul.moradi@iaukhsh.ac.ir

panels under axial compression and thermal load using the first-order shear deformation shell theory and element-free kp -Ritz method. Foroutan and Moradi-Dastjerdi (2011) applied a moving least square (MLS) based mesh-free method for dynamic analysis of isotropic FGM cylinders subjected to impact load. Ghadiri Rad *et al.* (2015) used MLPG method and hyper-elastic neo-Hookean model for nonlinear dynamic analysis of hyper-elastic FGM cylinder with Rayleigh damping. Also, about FG-CNTRC structures, Shen, 2011 studied on postbuckling analysis of FG-CNTRC cylindrical shells in thermal environments based on a singular perturbation technique. Yas and Heshmati (2012) applied Timoshenko and Euler–Bernoulli beam theories investigated the vibrational behavior of nanocomposite beams reinforced by functionally graded randomly oriented CNTs under a moving load. Lei *et al.* (2014) presented dynamic stability analysis of FG-CNTRC cylindrical panels based on element-free kp -Ritz method. Tahouneh and Naei (2016) presented free vibration behavior of aggregated CNTRC curve panels based on the three-dimensional theory of elasticity. They assumed the volume fractions of randomly oriented agglomerated CNTs to be graded along both the radial and axial directions of the curved panel. Moradi-Dastjerdi (2016), Moradi-Dastjerdi and Pourasghar (2016) used an MLS shape function based mesh-free method for analysis of stress wave propagations in nanocomposite cylinders reinforced by FG wavy and aggregated CNTs under impact loads. They also developed a mesh-free method and first order shear deformation theory (FSDT) to investigate vibrational and dynamic behavior of nanocomposite plates reinforced by wavy CNTs (Moradi-Dastjerdi and Momeni-Khabisi 2016, 2017). Using the element-free IMLS-Ritz method and FSDT, Zhang *et al.* (2016) analyzed on the elastodynamic behavior of quadrilateral FG-CNTRC plates subjected to a transverse sudden dynamic load.

The effect of thermal gradient loads has been considered in some research. Alibeigloo 2016; Alibeigloo and Liew, 2013 used 3D theory of elasticity presented thermoelastic static analysis of FG-CNTRC cylindrical panels and plates subjected to thermal gradient loads but with temperature independent material properties of CNT and polymer. Pourasghar and Chen (2016) studied on the three-dimensional thermoelastic static analyses of FG-CNTRC cylindrical panels, subjected to thermal gradient loads by Generalized Differential Quadrature (GDQ) method. They used suitable temperature and displacement functions to satisfy boundary conditions and to reduce the equilibrium equations as a set of coupled ordinary differential equations with variable coefficients. Moradi-Dastjerdi and Payganeh, 2017b considered axisymmetric FG-CNTRC cylinders which are subjected to thermal flux, convection environments and constant temperature faces and investigated transient heat transfer analysis of the cylinders. Finally, Moradi-Dastjerdi *et al.* (2016), Moradi-Dastjerdi and Payganeh (2017a) presented thermoelastic static and free vibration behavior of FG cylinders reinforced by single-walled wavy CNTs subjected to thermal gradient and mechanical loads. They used a micro mechanical model in volume fraction form to estimate temperature-dependent

mechanical properties of the nanocomposite.

In all the above mentioned works, thermoelastic dynamic analysis FG-CNTRC cylinders subjected to thermal gradient loads and with temperature-dependent material properties has not been yet considered and the present work attempts to consider thermal wave propagation analysis for FG nanocomposite cylinders reinforced by wavy CNT in presence of temperature gradient along the radial direction using a mesh-free method. In the mesh-free analysis, moving least squares shape functions are used to approximate temperature and displacement fields in the weak form of motion equation and transient thermal equation, respectively. Also, transformation method is used to impose their essential boundary conditions. This mesh-free method does not increase the calculations against Element-Free Galerkin (EFG). Material properties are estimated by a micro mechanical model. An uniformly and four linear types of FG distributions for nanotubes along the radial direction of cylinder are considered and the effects of thermal and mechanical loads, and also, waviness index, aspect ratio, volume fraction and distribution pattern of CNTs are investigated on wave propagations of FG-CNTRC cylinders.

2. Material properties in FG-CNTRC cylinders

The considered nanocomposite cylinders are made from a mixture of wavy SWCNT (along the radial direction) and matrix which is assumed to be isotropic. The wavy SWCNT reinforcement is either uniformly distributed (UD) or functionally graded in the radial direction. To obtain the mechanical properties of nanocomposites, a version of rule of mixture is applied that assumes the fibers are wavy and has uniform dispersion in the polymer matrix. This equation can't consider the length of fiber, so it can be modified by incorporating efficiency parameter (η^*) to account the nanotube aspect ratio (AR) and waviness (w) (Martone *et al.* 2011). The effective temperature-dependent material properties of the CNTRC cylinders are obtained based on a micromechanical model according to (Shen 2009)

$$E_1(T) = \eta_1 V_{CN} E_{1,\eta^*}(T) + V_m E^m(T) \quad (1)$$

$$\frac{\eta_2}{E_2(T)} = \frac{V_{CN}}{E_{2,\eta^*}(T)} + \frac{V_m}{E^m(T)} \quad (2)$$

$$\frac{\eta_3}{G_{12}(T)} = \frac{V_{CN}}{G_{12,\eta^*}(T)} + \frac{V_m}{G^m(T)} \quad (3)$$

$$\nu_{ij} = V_{CN} \nu_{ij}^{CN} + V_m \nu^m \quad i, j = 1, 2, 3 \text{ and } i \neq j \quad (4)$$

$$\rho = V_{CN} \rho^{CN} + V_m \rho^m, \quad c_p = V_{CN} c_p^{CN} + V_m c_p^m \quad (5)$$

$$\alpha_{11}(T) = V_{CN} \alpha_{11}^{CN}(T) + V_m \alpha^m(T) \quad (6)$$

$$\alpha_{22}(T) = (1 + \nu_{12}^{CN})V_{CN}\alpha_{22}^{CN}(T) + (1 + \nu^m)V_m\alpha^m(T) - \nu_{12}\alpha_{11}(T) \quad (7)$$

$$k_{11} = \eta_1 V_{CN} k_{11}^{CN} + V_m k^m \quad (8)$$

$$\frac{\eta_2}{k_{22}} = \frac{V_{CN}}{k_{11}^{CN}} + \frac{V_m}{k^m} \quad (9)$$

where

$$E_{i,\eta^*} = \eta^* E_i^{CN} \quad (10)$$

$$\eta^* = 1 - \frac{\tanh(K.AR/(1 + \langle c \rangle))}{K.AR/(1 + \langle c \rangle)}, \quad (11)$$

$$K = \sqrt{\frac{-2}{1 + \nu_m} \left/ \left(\frac{E^{CN}}{E^m} \ln(V_{CN}) \right) \right.}$$

and where E_i^{CN} , G_{12}^{CN} , ν^{CN} , E_{η^*} , $\langle c \rangle$, k_{ii}^{CN} , c_p^{CN} , ρ^{CN} and α_{ii}^{CN} are elasticity modulus, shear modulus, Poisson's ratio, effective reinforcement modulus, the average number of contacts per particle, thermal conductivity, specific heat conduction, mass density and thermal expansion coefficients in the longitudinal ($i=1$) and transverse ($i=2$) directions, respectively, of the carbon nanotube. E^m , G^m , ν^m , k^m , ρ^m and α^m are corresponding properties for the matrix. T is temperature, V_{CN} and V_m are the fiber (CNT) and matrix volume fractions and are related by $V_{CN} + V_m = 1$. η_j ($j=1,2,3$) are the CNT efficiency parameters and the applied values of η_1 and η_2 are listed in Table 1, in which taking $\eta_3 = 0.7\eta_2$ (Shen 2009).

It must be noticed that the average number of contacts, $\langle c \rangle$, for tubes is dependent on their aspect ratio (Martone *et al.* 2011)

$$\langle c \rangle = w.V_{CN} \cdot \left(4 + \frac{3AR^2}{3AR + 2} \right) \quad (12)$$

where the waviness index, w , has been introduced in order to account the CNTs curvature within the real composite.

Accordingly to literature (Martone *et al.* 2011), the variation of the excluded volume due to nanotubes curvature has been here investigated by introducing the waviness parameter, w .

The profile of the variation of fiber volume fraction has important effects on the cylinder behavior. In this paper four linear types (FG-V, FG- \wedge , FG-X and FG-O) are assumed for the distribution of CNT reinforcements along the radial direction in FG-CNTRC cylinder.

Table 1 (10,10) SWCNT efficiency parameter (Shen 2009)

V_{CN}^*	η_1	η_2
0.12	0.137	1.022
0.17	0.142	1.626
0.28	0.141	1.585

In this paper four linear types (FG-V, FG- \wedge , FG-X and FG-O) are assumed for the distribution of CNT reinforcements along the radial direction in FG-CNTRC cylinder.

$$V_{CN}^* = \frac{\rho^m}{\rho^m + (\rho^{CN}/w^{CN}) - \rho^{CN}} \quad (13)$$

and w^{CN} is the mass fraction of nanotube.

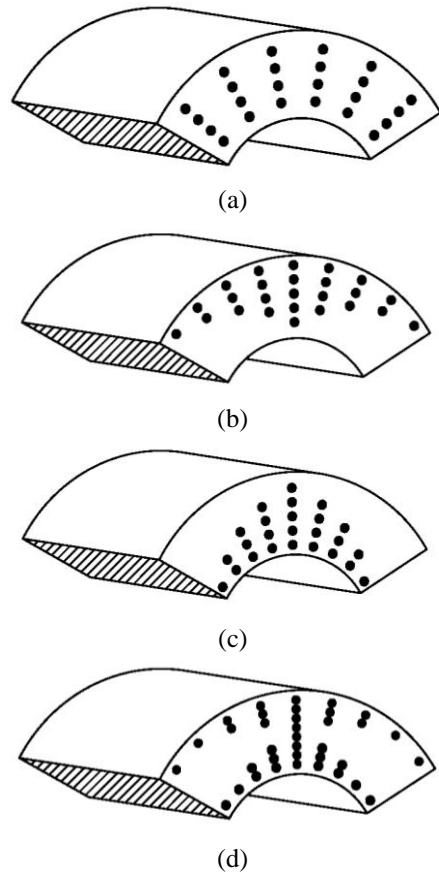


Fig. 1 Schematic of CNT distributions for (a) UD, (b) FG-V, (c) FG- \wedge and (d) FG-X

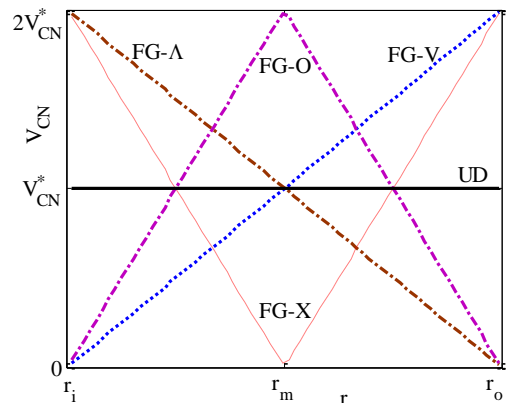


Fig. 2 Variation of CNT volume fraction (V_{CN}) along the radial direction

3. Governing equations

The transient heat conduction equation for axisymmetric FG distribution of CNT along the radial direction is taken as (Alibeigloo 2016)

$$k_r(r) \frac{\partial^2 T(r,z)}{\partial r^2} + \frac{\partial k_r(r)}{\partial r} \frac{\partial T(r,z)}{\partial r} + \frac{k_r(r)}{r} \frac{\partial T(r,z)}{\partial r} + k_z(z) \frac{\partial^2 T(r,z)}{\partial z^2} = \rho(r)c_p(r) \frac{\partial T(r,z)}{\partial t} \quad (14)$$

where $T(r, z)$ is the temperature at point $\mathbf{X} = \mathbf{X}_i(r, z)$.

By solving this equation, temperature distribution in FG-CNTRC cylinders can be derived.

Also, the weak form of motion equation in the absence of body forces is expressed as:

$$\int_{\Omega} \boldsymbol{\sigma} : \delta \boldsymbol{\varepsilon} dv - \int_{\Gamma} \mathbf{F} \cdot \delta \mathbf{u} ds = - \int_{\Omega} \rho(r) \ddot{\mathbf{u}} \cdot \delta \mathbf{u} dv \quad (15)$$

where \mathbf{F} , $\boldsymbol{\sigma}$, $\boldsymbol{\varepsilon}$, \mathbf{u} and $\ddot{\mathbf{u}}$ are surface traction, stress, strain, displacement and acceleration vectors, respectively. The deformations of structures can be happened by a mechanical loads or temperature gradient as elastic strains and thermal strains, respectively. So, the strain vectors are as: total strain vector, \mathbf{e} , elastic strain vector, $\boldsymbol{\varepsilon}$, and thermal strain vector, $\boldsymbol{\varepsilon}_T$. For axisymmetric problems stress and strain vectors are defined as follows

$$\boldsymbol{\sigma} = [\sigma_r, \sigma_\theta, \sigma_z, \sigma_{rz}]^T \quad (16)$$

$$\boldsymbol{\varepsilon} = [\varepsilon_r, \varepsilon_\theta, \varepsilon_z, \varepsilon_{rz}]^T \quad (17)$$

$$\boldsymbol{\varepsilon}_T = [\alpha \Delta T, \alpha \Delta T, \alpha \Delta T, 0]^T \quad (18)$$

where $\Delta T = T - T_0$ is and $T_0 = 300\text{K}$ (ambient temperature, where there are no thermal strains). The strain vectors are related by

$$\mathbf{e} = \boldsymbol{\varepsilon} + \boldsymbol{\varepsilon}_T \quad (19)$$

and the components of total strain vector are related to displacement vector components by the following relations

$$e_r = \frac{\partial u_r}{\partial r}, e_\theta = \frac{u_r}{r}, e_z = \frac{\partial u_z}{\partial z}, e_{rz} = \frac{\partial u_r}{\partial z} + \frac{\partial u_z}{\partial r} \quad (20)$$

Stress vector is expressed in terms of elastic strain vector as

$$\boldsymbol{\sigma} = \mathbf{D} \boldsymbol{\varepsilon} \quad (21)$$

For an orthotropic cylinder whose material axes of orthotropy coincide with axial, radial and circumferential directions, matrix \mathbf{D} is defined as follows

$$\mathbf{D} = \begin{bmatrix} c_{11}(r,T) & c_{12}(r,T) & c_{13}(r,T) & 0 \\ c_{12}(r,T) & c_{22}(r,T) & c_{23}(r,T) & 0 \\ c_{13}(r,T) & c_{23}(r,T) & c_{33}(r,T) & 0 \\ 0 & 0 & 0 & c_{55}(r,T) \end{bmatrix} \quad (22)$$

$$\begin{aligned} c_{11} &= \frac{1 - \nu_{23} \nu_{32}}{E_2 E_3 \Delta}, c_{22} = \frac{1 - \nu_{31} \nu_{13}}{E_1 E_3 \Delta}, c_{13} = \frac{\nu_{31} + \nu_{21} \nu_{32}}{E_2 E_3 \Delta}, c_{33} = \frac{1 - \nu_{21} \nu_{12}}{E_1 E_2 \Delta}, c_{12} = \frac{\nu_{21} + \nu_{31} \nu_{23}}{E_2 E_3 \Delta} \\ c_{23} &= \frac{\nu_{32} + \nu_{12} \nu_{31}}{E_1 E_3 \Delta}, c_{55} = G_{12}, \Delta = \frac{1 - \nu_{32} \nu_{23} - \nu_{21} \nu_{12} - \nu_{13} \nu_{31} - 2 \nu_{32} \nu_{21} \nu_{13}}{E_1 E_2 E_3} \end{aligned} \quad (21)$$

4. Mesh-free numerical analysis

In this paper, moving least square shape functions are used for approximation of displacement vector in the weak form of motion equation (Lancaster and Salkauskas 1981). Displacement vector \mathbf{u} can be approximated by MLS shape functions as follows

$$\mathbf{u} = [u_r, u_z]^T = \boldsymbol{\Phi} \hat{\mathbf{u}} \quad (24)$$

where $\hat{\mathbf{u}}$ and $\boldsymbol{\Phi}$ are virtual nodal values vector and shape functions matrix, respectively.

$$\hat{\mathbf{u}} = [(\hat{u}_r)_1, (\hat{u}_z)_1, \dots, (\hat{u}_r)_N, (\hat{u}_z)_N]^T \quad (25)$$

$$\boldsymbol{\Phi} = \begin{bmatrix} \Phi_1 & 0 & \Phi_2 & 0 & \dots & \Phi_N & 0 \\ 0 & \Phi_1 & 0 & \Phi_2 & \dots & 0 & \Phi_N \end{bmatrix} \quad (26)$$

and N is total number of nodes. By using Eq. (24) for approximation of displacement vector, strain vector can be expressed in terms of virtual nodal values

$$\boldsymbol{\varepsilon} = \mathbf{B} \hat{\mathbf{u}} \quad (27)$$

where matrix \mathbf{B} is defined as follows

$$\mathbf{B} = \begin{bmatrix} \frac{\partial \Phi_1}{\partial r} & 0 & \frac{\partial \Phi_2}{\partial r} & 0 & \dots & \frac{\partial \Phi_N}{\partial r} & 0 \\ \frac{\Phi_1}{r} & 0 & \frac{\Phi_2}{r} & 0 & \dots & \frac{\Phi_N}{r} & 0 \\ 0 & \frac{\partial \Phi_1}{\partial z} & 0 & \frac{\partial \Phi_2}{\partial z} & \dots & 0 & \frac{\partial \Phi_N}{\partial z} \\ \frac{\partial \Phi_1}{\partial z} & \frac{\partial \Phi_1}{\partial r} & \frac{\partial \Phi_2}{\partial z} & \frac{\partial \Phi_2}{\partial r} & \dots & \frac{\partial \Phi_N}{\partial z} & \frac{\partial \Phi_N}{\partial r} \end{bmatrix} \quad (28)$$

Substitution of Eq. (21), Eq. (24) and Eq. (27) in Eq. (15) leads to

$$\mathbf{M} \ddot{\hat{\mathbf{u}}} + \mathbf{k} \hat{\mathbf{u}} = \mathbf{f} \quad (29)$$

where

$$\mathbf{M} = \int_{\Omega} \rho \boldsymbol{\Phi}^T \boldsymbol{\Phi} dv, \mathbf{k} = \int_{\Omega} \mathbf{B}^T \mathbf{D} \mathbf{B} dv, \mathbf{f} = \int_{\Gamma} \boldsymbol{\Phi}^T \mathbf{F} ds \quad (30)$$

For numerical integration, problem domain is discretized to a set of background cells with Gauss points inside each cell. Then global stiffness matrix, \mathbf{k} , and mass matrix, \mathbf{M} , are obtained numerically by sweeping all Gauss points inside Ω .

Imposition of essential boundary conditions in the system of Eq. (29) is not possible. Because MLS shape functions don't satisfy the Kronecker delta property. In this work transformation method is used for imposition of essential boundary conditions. For this purpose, transformation matrix is formed by establishing relation

between nodal displacement vector \mathbf{U} and virtual displacement vector $\hat{\mathbf{u}}$.

$$\mathbf{U} = \mathbf{T}\hat{\mathbf{u}} \quad (31)$$

\mathbf{T} is the transformation matrix.

$$\mathbf{T} = \begin{bmatrix} \Phi_1(\mathbf{x}_1) & 0 & \Phi_2(\mathbf{x}_1) & 0 & \dots & \Phi_N(\mathbf{x}_1) & 0 \\ 0 & \Phi_1(\mathbf{x}_1) & 0 & \Phi_2(\mathbf{x}_1) & \dots & 0 & \Phi_N(\mathbf{x}_1) \\ \vdots & \vdots & \vdots & \vdots & \ddots & \vdots & \vdots \\ \Phi_1(\mathbf{x}_N) & 0 & \Phi_2(\mathbf{x}_N) & 0 & \dots & \Phi_N(\mathbf{x}_N) & 0 \\ 0 & \Phi_1(\mathbf{x}_N) & 0 & \Phi_2(\mathbf{x}_N) & \dots & 0 & \Phi_N(\mathbf{x}_N) \end{bmatrix} \quad (32)$$

By using Eq. (31) system of linear Eq. (29) can be rearranged to

$$\hat{\mathbf{M}}\ddot{\mathbf{U}} + \hat{\mathbf{k}}\mathbf{U} = \mathbf{f} \quad (33)$$

where

$$\hat{\mathbf{M}} = \mathbf{T}^{-T}\mathbf{M}\mathbf{T}^{-1}, \quad \hat{\mathbf{k}} = \mathbf{T}^{-T} \cdot \mathbf{k} \cdot \mathbf{T}^{-1}, \quad \hat{\mathbf{f}} = \mathbf{T}^{-T} \cdot \mathbf{f} \quad (34)$$

Now the essential B. Cs. can be enforced to the modified equations system (Eq. (33)) easily like the finite element method. In this work, the Newmark (central difference) method is used for solution of this equation in time domain.

By the same method, mesh-free formulation for transient thermal equation can be defined as

$$\mathbf{C} \frac{d\hat{\mathbf{T}}}{dt} + \mathbf{K}_T \hat{\mathbf{T}} = \mathbf{q} \quad (35)$$

where \mathbf{C} , \mathbf{k}_T , $\hat{\mathbf{T}}$ and \mathbf{q} are thermal mass matrix, thermal stiffness matrix, virtual temperature vector and flux vector, respectively and are defined as

$$\mathbf{C} = \int_{\Omega} (\rho c_p) \Phi^T \Phi dv, \quad \mathbf{k}_T = \int_{\Omega} \mathbf{B}_T^T \mathbf{D}_T \mathbf{B}_T dv, \quad \mathbf{q} = \int_{\Gamma} \Phi^T \mathbf{Q} ds, \quad \hat{\mathbf{T}} = [T_1 \quad T_2 \quad \dots \quad T_N]^T \quad (36)$$

and where

$$\Phi_T = \begin{bmatrix} \Phi_1 \\ \Phi_1 \\ \vdots \\ \Phi_N \end{bmatrix}, \quad \mathbf{B}_T = \begin{bmatrix} \frac{\partial \Phi_1}{\partial r} & \frac{\partial \Phi_2}{\partial r} & \dots & \frac{\partial \Phi_N}{\partial r} \\ \frac{\partial \Phi_1}{\partial z} & \frac{\partial \Phi_2}{\partial z} & \dots & \frac{\partial \Phi_N}{\partial z} \end{bmatrix}, \quad \mathbf{D}_T = \begin{bmatrix} k_r(r) & 0 \\ 0 & k_z(r) \end{bmatrix} \quad (37)$$

Also, the transformation matrix for the thermal equation and the relation between nodal temperature vector, \mathbf{Temp} , and virtual temperature vector, $\hat{\mathbf{T}}$, can be defined as

$$\mathbf{Temp} = \mathbf{R} \hat{\mathbf{T}}, \quad \mathbf{R} = \begin{bmatrix} \Phi_1(\mathbf{X}_1) & \Phi_2(\mathbf{X}_1) & \dots & \Phi_N(\mathbf{X}_1) \\ \Phi_1(\mathbf{X}_2) & \Phi_2(\mathbf{X}_2) & \dots & \Phi_N(\mathbf{X}_2) \\ \vdots & \vdots & \ddots & \vdots \\ \Phi_1(\mathbf{X}_N) & \Phi_2(\mathbf{X}_N) & \dots & \Phi_N(\mathbf{X}_N) \end{bmatrix} \quad (38)$$

5. Results and discussions

In this section, at first the accuracy of applied method is

examined. Then, thermoelastic dynamic behavior of the nanocomposite cylinders reinforced by wavy CNTs and subjected to mechanical or thermal loads are investigated. For this purpose, the material properties and stress wave propagation of the nanocomposite cylinders are derived after solving of transient thermal equation and obtaining of the time history of temperature field of the cylinders. It can be considered that, the polymer and CNT material properties are assumed temperature dependent. The effects of waviness, distribution pattern and volume fraction of CNT, temperature of environment and direction of thermal gradient loads are investigated on the thermoelastic dynamic behavior of FG-CNTRC cylinders.

In the following simulations, CNTRC cylinders are considered made of Poly (methyl- methacrylate, referred as PMMA) as matrix and wavy CNT as fiber. PMMA is an isotropic material with $\nu^m = 0.34$, $c_p = 1466(j/Kg.K)$,

$\rho^m = 1150 Kg/m^3$ and $k^m = 0.247 W/mK$ but temperature dependent elasticity modulus and thermal expansion coefficients as (Pourasghar et al., 2016; Shen, 2011):

$$E^m = (3.52 - 0.0034T) GPa, \quad (38)$$

$$\alpha^m = 45(1 + 0.0005 \Delta T) \times 10^{-6} / K$$

so, $E^m = 2.5 GPa$ and $\alpha^m = 45 \times 10^{-6} / K$ are at ambient temperature ($T_0 = 300 K$). The properties of armchair (10, 10) configuration of SWCNTs ($L=9.26 nm$, $R=0.68 nm$, $h=0.067 nm$) are taken same as Table 2 at some temperatures (Pourasghar et al. 2016; Shen 2011). So by considering of the values of Table 2 which are reported at four temperatures, the CNT material properties are estimated by separate polynomials of degree three as

$$P = P_1 T^3 + P_2 T^2 + P_3 T + P_4 \quad (39)$$

where P is used for temperature dependent material properties of CNT and P_i ($i=1,2,3,4$) are the constant values and they are determined in Table 3. The other properties of CNT are assumed temperature independent and equal to, $\rho^{CN} = 1400 Kg/m^3$, $c_p = 600(j/Kg.K)$ and $\nu^{CN} = 0.175$.

For convenience, the normalized physical quantities are defined by

$$\bar{\sigma} = \frac{\sigma}{E \alpha T_0}, \quad \bar{U} = \frac{U}{r_o \alpha T_0}, \quad \bar{T} = \frac{T}{T_0} \quad (41)$$

5.1 Validation models

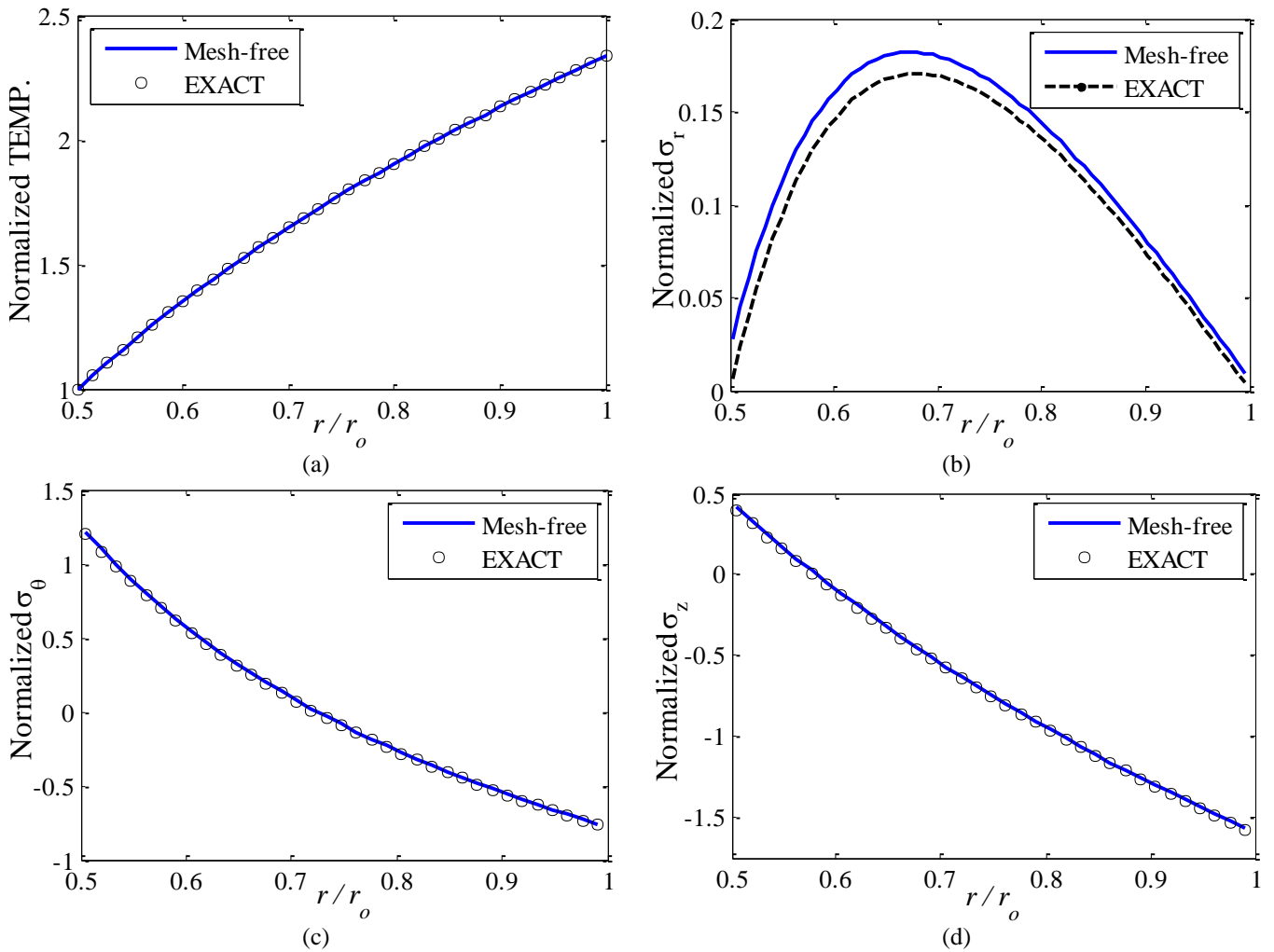
For validation of the proposed mesh-free method, at first, the steady state distributions of stresses and temperature are examined in a long homogeneous cylinder (plane strain state) with the internal temperature of, T_i , and external of, T_o .

Table 2 Material properties of (10,10) SWCNT (Shen 2011)

T (K)	E_{11}^{CN} (GPa)	E_{22}^{CN} (GPa)	G_{12}^{CN} (GPa)	α_{11}^{CN} ($10^{-6}/K$)	α_{22}^{CN} ($10^{-6}/K$)	k_{11}^{CN} (W/mK)	k_{22}^{CN} (W/mK)
300	5646.6	7080	1944.5	3.4584	5.1682	3000	100
400	5667.9	6981.4	1970.3	4.1496	5.0905	3000	100
500	5530.8	6934.8	1964.3	4.5361	5.0189	3000	100
700	5474.4	6864.1	1964.4	4.6677	4.8943	3000	100

Table 3 Constant values for material properties of temperature dependent CNT

P	P_1	P_2	P_3	P_4
E_{11}^{CN}	-4.4583e3	7.4300e6	-4.3384e9	6.3998e12
E_{22}^{CN}	-5.5625e3	9.2750e6	-5.4204e9	8.0216e12
G_{12}^{CN}	4.4792e3	-6.9650e6	3.4762e9	1.4076e12
α_{11}^{CN}	1.1363e-14	-2.8870e-11	2.2917e-08	-1.1252e-6
α_{22}^{CN}	1.2500e-17	2.9000e-13	-9.8463e-10	5.4372e-6

Fig. 3 Comparison of (a) \bar{T} , (b) $\bar{\sigma}_r$, (c) $\bar{\sigma}_\theta$ and (d) $\bar{\sigma}_z$ distributions along the cylinder thickness

Figs. 3 show excellent agreements between the results of applied mesh-free method and exact solution (Hetnarski and Eslami 2009) for the distributions of normalized temperature, \bar{T} , radial stress, $\bar{\sigma}_r$, hoop stress, $\bar{\sigma}_\theta$, and axial stress, $\bar{\sigma}_z$, in a the cylinder. It can be seen that cylinder temperature is smoothly varied from T_i to T_o along the radial direction. This trend can be seen for hoop and axial stresses where inner radius has the highest values of ones. Because of the inner and outer surfaces of cylinder are traction free, it is observed that their values of radial stresses are zero and the highest value of radial between them.

Now, consider CNTRC cylinders with inner radius of, $r_i = 0.18m$, outer radius of, $r_o = 0.2m$, length of, $L = 0.2m$, CNT volume fraction of, $V_{CN}^* = 0.17$, initial temperatures, $T^0 = 300K$, isolated top and bottom ends, inner temperature of $T_i = 500K$ and outer temperature of $T_o = 300K$. Fig. 4(a) shows time histories of temperatures in the UD and FG-CNTRC cylinders at mid radius.

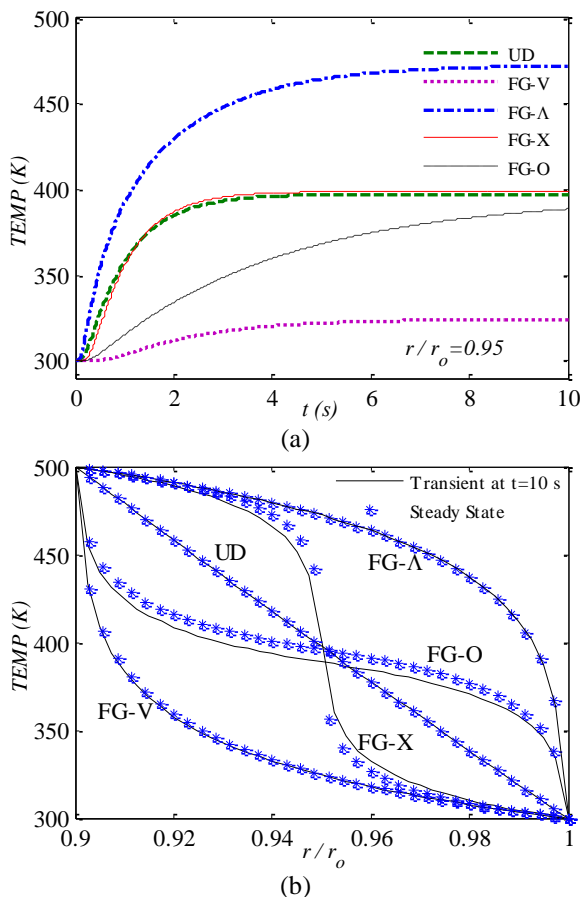


Fig. 4 Transient heat transfer responses of CNTRC cylinders with $r_i = 0.18m$, $r_o = 0.2m$, $L = 0.2m$, $V_{CN}^* = 0.17$, $T_i = 500K$, $T_o = 300K$ and isolated ends (a) time history of temperatures and (b) temperature along the radial direction

Because of CNT distribution and higher values of CNT thermal conductivity, it's observed UD and X cylinders get stationary condition before $t = 4s$ while O-CNTRC cylinder does not get it until $t = 10s$. Fig. 4(b) compares the steady state results of the cylinders and transient responses of them at $t = 10s$. It can be seen that UD, V and \wedge -CNTRC cylinders have mostly same temperature distributions in both cases of steady state and transient state after 10 seconds. But X and O cylinder types, because of a sharp variation in CNT distribution at mid radius, have little differences between their results of steady state and transient responses at $t = 10s$. Also, it's observed CNT distribution has a significant effect on the thermal behaviors of the nanocomposite cylinders.

5.2 Thermoelastic stress wave propagations in FG-CNTRC cylinders

For thermoelastic dynamic analysis, consider long X-CNTRC cylinders with $r_i = 0.16$, $r_o = 0.2$, $V_{CN}^* = 0.17$, $AR = 1000$, $w = 1$ and $T^0 = 300K$ that is equal to room temperature. The cylinders are subjected to mechanical (impact internal pressure) load as Eq. (42) or thermal loads as thermal environment of $T_{env} = 350K$ or $T_{env} = 400K$.

$$P(t) = P_0 \sin\left(\frac{\pi t}{0.12}\right) \quad \text{for } t \leq 0.12 \text{ (ms)} \quad (42)$$

$$P(t) = 0 \quad \text{for } t > 0.12 \text{ (ms)}$$

where $P_0 = 20$ MPa. Figs. 5 illustrate time histories of normalized hoop, radial and axial stresses and also normalized time history of radial displacement at mid radius of the cylinders. It can be seen that stress wave propagations of mechanical load are more methodical than those one of thermal loading. Also, the values of radial displacement and hoop stress due to mechanical loading are more than the correspond values due to thermal loading. Increasing of the temperature environment increases the values of stresses and displacement but decreases their propagation speeds.

Figs. 6 show time histories of normalized stresses and radial displacement at mid radius of the long X-CNTRC cylinders with $r_i = 0.16$, $r_o = 0.2$, $AR = 1000$, $T^0 = 300K$ and $T_{env} = 400K$ for different values of CNT waviness indexes and volume fractions. It can be seen that increasing of CNT waviness or volume value increases the values of stresses and their propagation speeds. The effect of CNT volume on the thermoelastic dynamic behavior of the cylinders is more than CNT waviness. Increasing of CNT volume leads to decreasing in the values of displacement and increasing in their propagation speeds. It's observed that the values of radial stresses are more than the others stresses.

Finally, the effect of thermal gradient loads on the thermoelastic dynamic behavior of CNTRC cylinders is investigated. Consider UD and X-CNTRC cylinders with

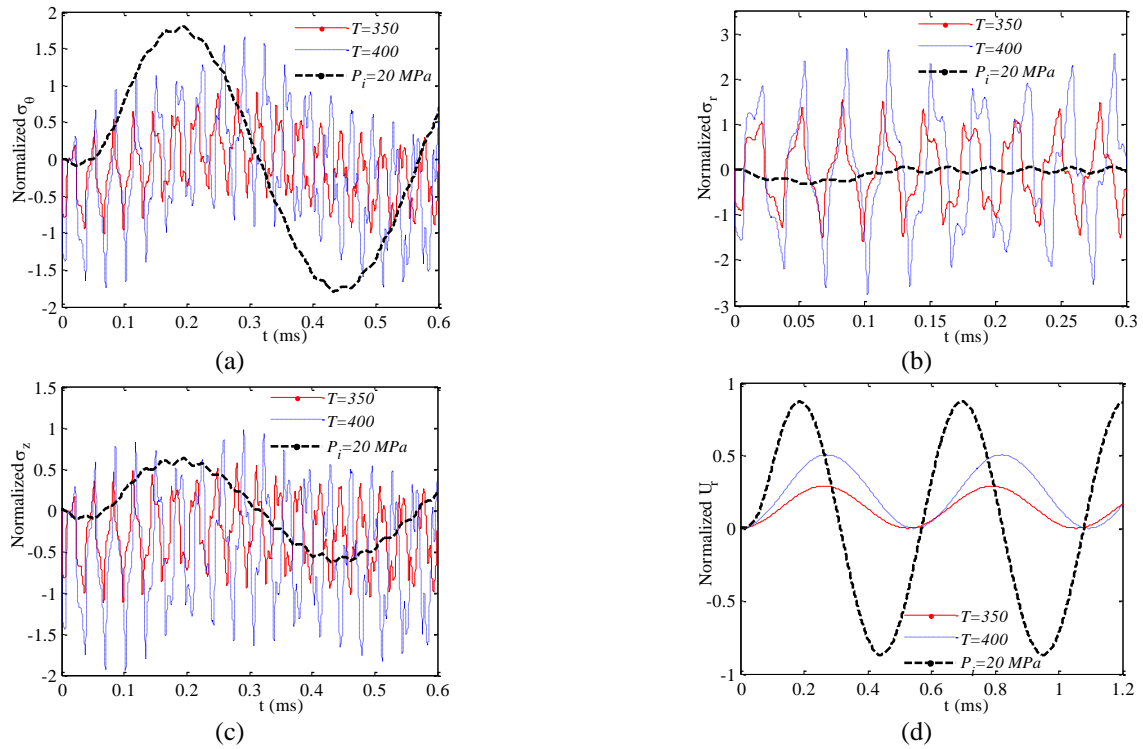


Fig. 5 Time histories of (a) $\bar{\sigma}_\theta$, (b) $\bar{\sigma}_r$, (c) $\bar{\sigma}_z$ and (d) \bar{U}_r at mid radius of long X-CNTRC cylinders with $r_i = 0.16$, $r_o = 0.2$, $V_{CN}^* = 0.17$, $AR = 1000$ and $w = 1$

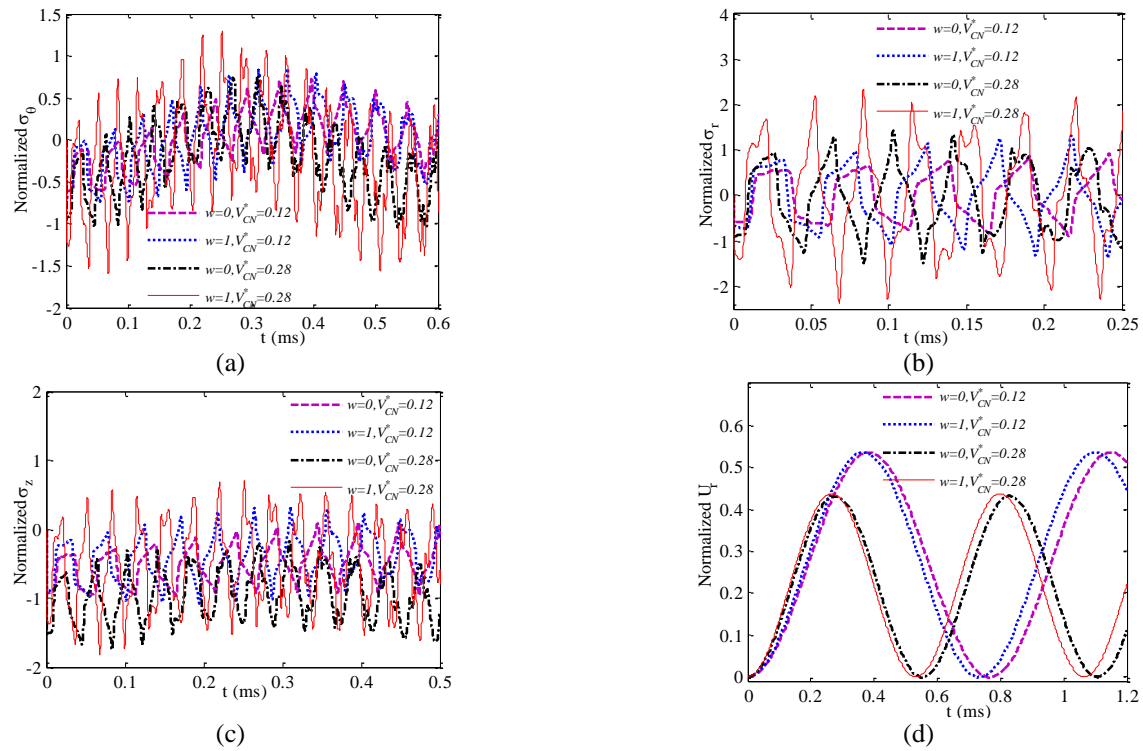


Fig. 6 Time histories of (a) $\bar{\sigma}_\theta$, (b) $\bar{\sigma}_r$, (c) $\bar{\sigma}_z$ and (d) \bar{U}_r at mid radius of long X-CNTRC cylinders with $r_i = 0.16$, $r_o = 0.2$, $AR = 1000$, $T^0 = 300 K$ and $T_{env} = 400 K$

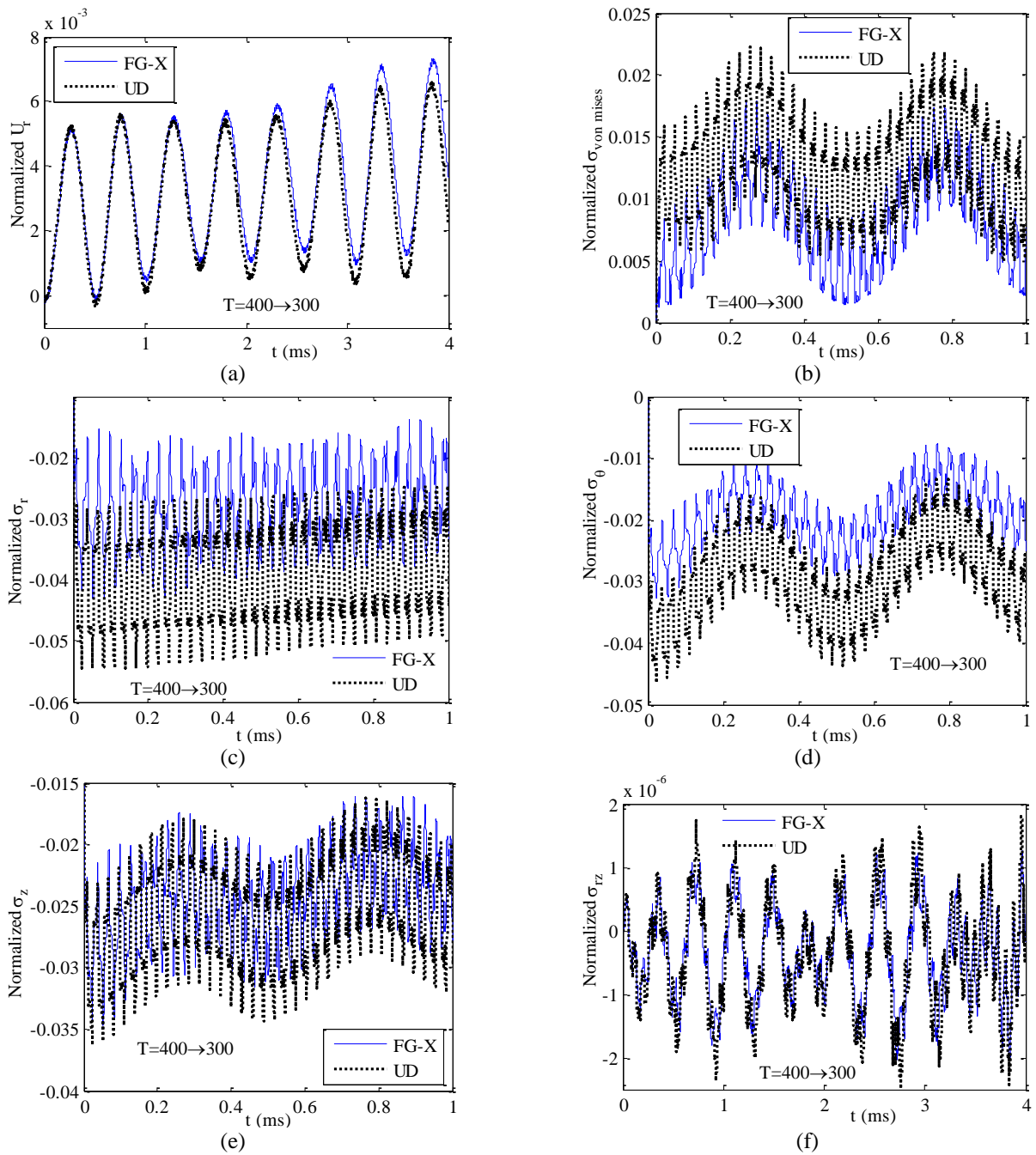


Fig. 7 Time histories of (a) \bar{U}_r , (b) $\bar{\sigma}_{\text{vMises}}$, (c) $\bar{\sigma}_r$, (d) $\bar{\sigma}_\theta$, (e) $\bar{\sigma}_z$ and (f) $\bar{\sigma}_{rz}$ at mid radius of CNTRC cylinders with $r_i = 0.16$, $r_o = 0.2$, $V_{CN}^* = 0.17$, $w = 1$, $AR = 1000$, $T^0 = 300 K$ subjected to incoming thermal gradient

$r_i = 0.16$, $r_o = 0.2$, $V_{CN}^* = 0.17$, $AR = 1000$, $w = 1$, $T^0 = 300 K$ and thermal isolated ends. Figs 7 and 8 show time histories of radial displacement and stresses for two kinds of temperature boundary conditions of $T_i = 400 K$, $T_o = 300 K$ (incoming thermal gradient) and $T_i = 300 K$, $T_o = 400 K$ (outgoing thermal gradient), respectively. It can be seen that the values of displacements in X-types of

CNTRC cylinders are more than UD ones but their propagation speeds are a little less than UD ones and incoming thermal gradient leads to higher values of displacement. In both temperature boundary conditions, the stress values of X-CNTRC cylinders are less than UD cylinders and outgoing thermal gradient leads to more values of stresses in cylinders. In these cylinders, radial and shear stresses have the biggest and smallest values of stresses, respectively.

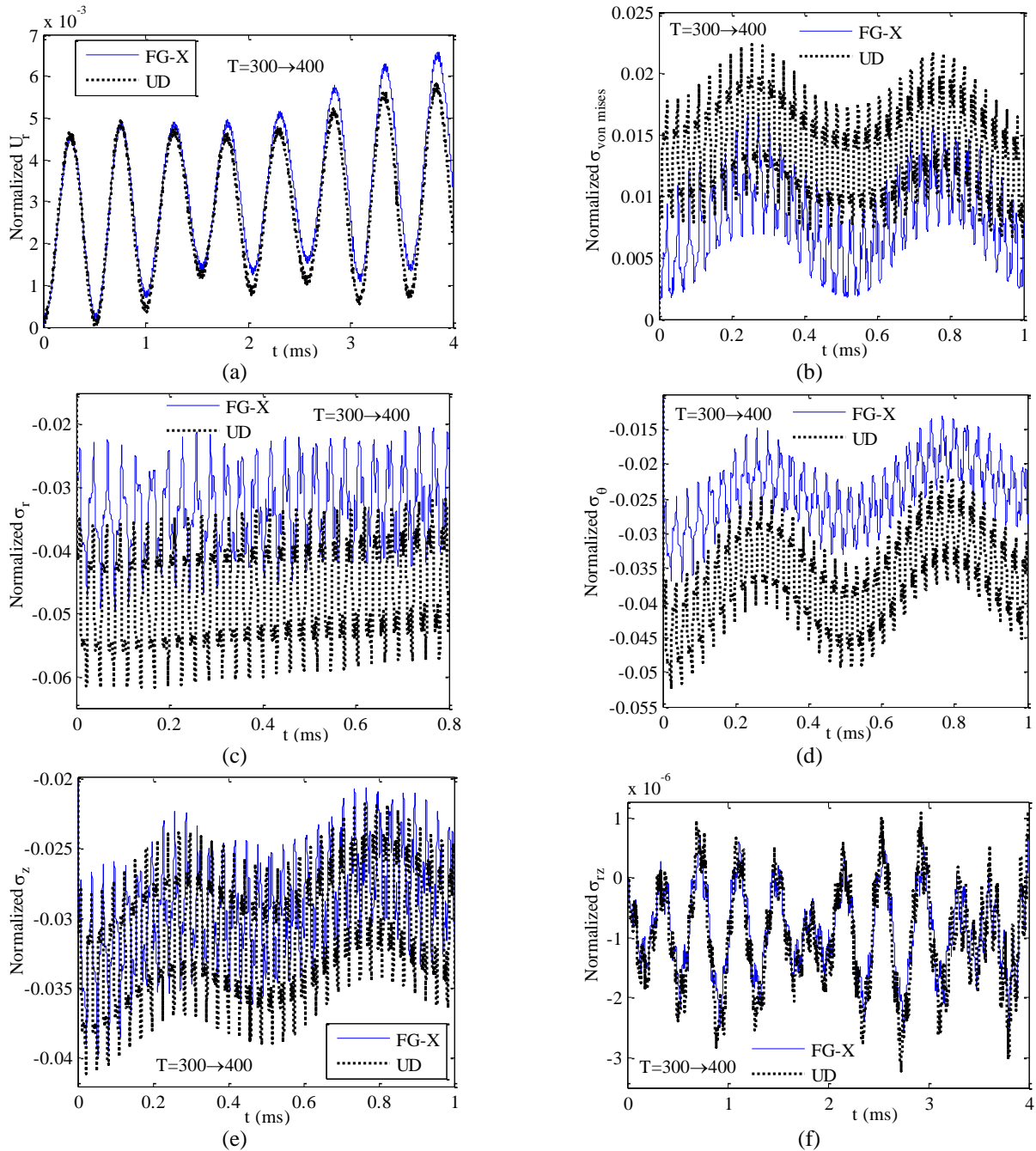


Fig. 8 Time histories of (a) \bar{U}_r , (b) $\bar{\sigma}_{\text{von mises}}$, (c) $\bar{\sigma}_r$, (d) $\bar{\sigma}_\theta$, (e) $\bar{\sigma}_z$ and (f) $\bar{\sigma}_{rz}$ at mid radius of CNTRC cylinders with $r_i = 0.16$, $r_o = 0.2$, $V_{CN}^* = 0.17$, $w = 1$, $AR = 1000$, $T^0 = 300 K$ subjected to outgoing thermal gradient

6. Conclusions

In this work, the temperature-dependent material properties and stress wave propagations of the nanocomposite cylinders were derived after solving of the transient thermal equation and obtaining of time history of temperature field in cylinders subjected to impact pressure loads, uniform temperature environment or thermal gradient loads using the developed mesh-free method. Effects of distribution, volume fraction and waviness of CNT and also

thermal boundary conditions of cylinders were investigated on the overall thermoelastic dynamic behavior of the nanocomposite cylinders. The following results were obtained from this analysis:

- The developed mesh-free method has an excellent accuracy for thermoelastic dynamic analysis of the FG-CNTRC cylinders.
- CNT distribution has a significant effect on the thermal behaviors of the nanocomposite cylinders
- The values of radial displacement and hoop stress due

to mechanical loading are more than the correspond values due to thermal loading.

- Increasing of the temperature environment increases the values of stresses and displacement but decreases their propagation speeds.
- The effect of CNT volume on the thermoelastic dynamic behavior of the cylinders is more than CNT waviness.
- Incoming thermal gradient leads to higher values of displacement than outgoing ones.
- In Cylinders subjected to thermal gradient loads, the radial and shear stresses have the biggest and smallest values of stresses, respectively.

References

- Alibeigloo, A. (2016), "Elasticity solution of functionally graded carbon nanotube-reinforced composite cylindrical panel subjected to thermo mechanical load", *Compos. Part B*, **87**, 214–226.
- Alibeigloo, A. and Liew, K.M. (2013), "Thermoelastic analysis of functionally graded carbon nanotube-reinforced composite plate using theory of elasticity", *Compos. Struct.*, **106**, 873–881.
- Foroutan, M. and Moradi-Dastjerdi, R. (2011), "Dynamic analysis of functionally graded material cylinders under an impact load by a mesh-free method", *Acta Mech.*, **219**(3-4), 281–290.
- Ghadiri Rad, M.H., Shahabian, F. and Hosseini, S.M. (2015), "A meshless local Petrov – Galerkin method for nonlinear dynamic analyses of hyper-elastic FG thick hollow cylinder", *Acta Mech.*, **1513**, 1497-1513.
- Golbahar Haghighi, M.R., Eghtesad, M., Malekzadeh, P. and Neculescu, D.S. (2009), "Three-dimensional inverse transient heat transfer analysis of thick functionally graded plates", *Energ. Convers.Manage.*, **50**(3), 450-457.
- Hetnarski, R.B. and Eslami, M.R. (2009), *Thermal stresses–advanced theory and applications*, In: The Netherlands: Springer.
- Kundalwal, S. and Ray, M. (2013), "Effect of carbon nanotube waviness on the elastic properties of the fuzzy fiber reinforced composites", *J. Appl. Mech.*, **80**(2), 21010.
- Kundalwal, S.I. and Meguid, S.A. (2015), "Effect of carbon nanotube waviness on active damping of laminated hybrid composite shells. *Acta Mechanica* 226: 2035–2052.
- Kundalwal SI and Ray MC (2011) Micromechanical analysis of fuzzy fiber reinforced composites", *Int. J. Mech. Mater. Des.*, **7**(2), 149-166.
- Kundalwal, S.I. and Ray, M.C. (2014), "Improved thermoelastic coefficients of a novel short fuzzy fiber-reinforced composite with wavy carbon nanotubes", *J. Mech. Mater. Struct.*, **9**(1), 1-25.
- Kundalwal, S.I., Kumar, R.S. and Ray, M.C. (2014), "Effective thermal conductivities of a novel fuzzy carbon fiber heat exchanger containing wavy carbon nanotubes", *Int. J. Heat Mass Tran.*, **72**, 440-451.
- Lancaster, P. and Salkauskas, K. (1981), "Surface generated by moving least squares methods", *Math. Comput.*, **37**, 141-158.
- Lei, Z.X., Zhang, L.W., Liew, K.M. and Yu, J.L. (2014), "Dynamic stability analysis of carbon nanotube-reinforced functionally graded cylindrical panels using the element-free kp-Ritz method", *Compos. Struct.*, **113**, 328-338.
- Martone, A., Faiella, G., Antonucci, V., Giordano, M. and Zarrelli, M. (2011), "The effect of the aspect ratio of carbon nanotubes on their effective reinforcement modulus in an epoxy matrix", *Compos. Sci. Technol.*, **71**(8), 1117-1123.
- Mokashi, V., Qian, D. and Liu, Y. (2007), "A study on the tensile response and fracture in carbon nanotube-based composites using molecular mechanics", *Compos. Sci. Technol.*, **67**(3-4), 530-540.
- Moradi-Dastjerdi, R. (2016), "Wave propagation in functionally graded composite cylinders reinforced by aggregated carbon nanotube", *Struct. Eng. Mech.*, **57**(3), 441-456.
- Moradi-Dastjerdi, R. and Momeni-Khabisi, H. (2016), "Dynamic analysis of functionally graded nanocomposite plates reinforced by wavy carbon nanotube", *Steel Compos. Struct.*, **22**(2), 277-299.
- Moradi-Dastjerdi, R. and Momeni-Khabisi, H. (2017), "Vibrational behavior of sandwich plates with functionally graded wavy carbon nanotube-reinforced face sheets resting on Pasternak elastic foundation", *J. Vib. Control*, DOI: 10.1177/1077546316686227
- Moradi-Dastjerdi R and Payganeh G (2017a) Thermoelastic Vibration Analysis of Functionally Graded Wavy Carbon Nanotube-Reinforced Cylinders. *Polymer Composites*. DOI: 10.1002/pc.24278.
- Moradi-Dastjerdi, R. and Payganeh, G. (2017b), "Transient heat transfer analysis of functionally graded CNT reinforced cylinders with various boundary conditions", *Steel Compos. Struct.*, **24**(3), 359-367.
- Moradi-Dastjerdi, R. and Pourasghar, A. (2016), "Dynamic analysis of functionally graded nanocomposite cylinders reinforced by wavy carbon nanotube under an impact load", *J. Vib. Control*, **22**, 1062-1075.
- Moradi-Dastjerdi, R., Payganeh, G. and Tajdari, M. (2016), "Resonance in functionally graded nanocomposite cylinders reinforced by wavy carbon nanotube", *Polym. Compos.*, DOI: 10.1002/pc.24045
- Pourasghar, A. and Chen, Z. (2016), "Thermoelastic response of CNT reinforced cylindrical panel resting on elastic foundation using theory of elasticity", *Compos. Part B: Eng.*, **99**, 436-444.
- Pourasghar, A., Moradi-Dastjerdi, R., Yas M.H., Ghorbanpour Arani, A. and Kamarian, S. (2016), "Three-dimensional analysis of carbon nanotube- reinforced cylindrical shells With temperature- dependent properties under thermal environment", *Polym. Composit.*, DOI: 10.1002/pc.24046
- Qian, D., Dickey, E., Andrews, R. and Rantell, T. (2000), "Load transfer and deformation mechanisms in carbon nanotube– polystyrene composites", *Appl. Phys. Lett.*, **76**(20), 2868-2870.
- Ray, M.C. and Kundalwal, S.I. (2014), "A thermomechanical shear lag analysis of short fuzzy fiber reinforced composite containing wavy carbon nanotubes", *Eur. J. Mech. A-Solid*, **44**, 41-60.
- Shariyat, M., Khaghani, M. and Lavasani, S.M.H. (2010), "Nonlinear thermoelasticity, vibration, and stress wave propagation analyses of thick FGM cylinders with temperature-dependent material properties", *Eur. J. Mech. A-Solid*, **29**(3), 378-391.
- Shen, H. (2009), "Nonlinear bending of functionally graded carbon nanotube-reinforced composite plates in thermal environments", *Compos. Struct.*, **91**(1), 9-19.
- Shen, H. (2011), "Postbuckling of nanotube-reinforced composite cylindrical shells in thermal environments Part I: Axially-loaded shells", *Compos. Struct.*, **93**(8), 2096-2108.
- Sladek, J., Sladek, V., Hellmich, C.H. and Eberhardsteiner, J. (2007), "Heat conduction analysis of 3-D axisymmetric and anisotropic FGM bodies by meshless local Petrov – Galerkin method", *Comput. Mech.*, **39**(3), 323-333.
- Sofiyev, A.H. (2010), "Dynamic response of an FGM cylindrical shell under moving loads", *Compos. Struct.*, **93**(1), 58-66.
- Tahounh, V. and Naei, M.H. (2016), "3D free vibration analysis of elastically supported thick nanocomposite curved panels with finite length and different boundary conditions via 2-D GDQ

- method”, *Mech. Adv. Mater. Struct.*, **23**(10), 1216-1235.
- Yas, M.H. and Heshmati, M. (2012), “Dynamic analysis of functionally graded nanocomposite beams reinforced by randomly oriented carbon nanotube under the action of moving load”, *Appl. Math. Model.*, **36**(4), 1371-1394.
- Yazdchi, K. and Salehi, M. (2011), “The effects of CNT waviness on interfacial stress transfer characteristics of CNT / polymer composites”, *Compos. Part A*, **42**(10), 1301-1309.
- Zhang, L.W., Xiao, L.N., Zou, G.L. and Liew, K.M. (2016), “Elastodynamic analysis of quadrilateral CNT-reinforced functionally graded composite plates using FSDT element-free method”, *Compos. Struct.*, **148**, 144-154.
- Zhao, X. and Liew, K.M. (2010), “A mesh-free method for analysis of the thermal and mechanical buckling of functionally graded cylindrical shell panels”, *Comput. Mech.*, **45**(4), 297-310.
- Zhu, R., Pan, E. and Roy, A. (2007), “Molecular dynamics study of the stress-strain behavior of carbon-nanotube reinforced Epon 862 composites”, *Mater. Sci. Eng. A.*, **447**(1-2), 51-57.